City Research Online

City, University of London Institutional Repository

This is the published version of the paper.

This version of the publication may differ from the final published version.

Permanent repository link: https://openaccess.city.ac.uk/id/eprint/4415/

Link to published version:

3D CFD analysis of a twin screw expander

A Kovacevic, S Rane
City University London,
Centre for Positive Displacement Compressor Technology, UK

ABSTRACT

Twin screw machines can be used as expanders for variety of applications. This paper describes how the performance of an oil free twin screw air expander of 3/5 lobe configuration was estimated by use of full 3D Computational Fluid Dynamics (CFD) applying a procedure similar to that used for screw compressors. The grid generator SCORG© was employed for pre-processing of the moving domains between the rotors while the stationary grids for the ports were derived from a commercial grid generator. Flow calculations were carried out using the ANSYS CFX® solver. Pressure-angle diagrams, mass flow rates and expansion power at different operating conditions were estimated and compared with experimental test results. The overall performance predictions obtained by simulation agreed very well with measured data. It was concluded that correct design of the high pressure port is vital in order to obtain optimum power output. Leakage flows have a significant effect on screw expander efficiency and have the greatest influence at low speeds and high filling pressures.

ABBREVIATIONS

CFD – Computational Fluid Dynamics
FVM – Finite Volume Method
FEM – Finite Element Method
GGI – Generalized Grid Interface

SCORG© – Screw Compressor Rotor Grid Generator
ORC – Organic Rankine Cycle

1   INTRODUCTION

Twin screw expanders are positive displacement machines that can be used to recover mechanical power from fluids. Their expansion efficiency depends on several factors that include the leakage flows, the size and shape of the high pressure port and the volume ratio of the machine, as reported by *Smith et al.* (1). The analysis of such machines has been reported in several papers by *Stosic, Smith and Kovacevic* (2), (3) using a quasi 1D thermodynamic model. A detailed review of the methods used in the mathematical modelling of screw machines has been presented by *Stosic et al.* (4). *Bruemmer* and *Hutker,* (5), (6), more recently used a zero dimensional chamber model, based on the conservation of mass and energy, to predict the performance of such machines, in order to evaluate the influence of internal volume ratio V_i, length to diameter (L/D) ratio, rotor wrap angle Φ_w, size of leakage path and some other parameters. Similarly, *Nikolov et al.* (7), estimated the influence of rotor and casing thermal deformation on the performance of a screw expander in an ORC system, based on the iterative coupling of a thermodynamic chamber model and FEM thermal analysis.

The use of three dimensional transient CFD analyses of twin screw compressors is based on the conservation of energy, momentum and space for deforming domains by use of the finite volume method, the principles of which are extensively elaborated in (8). The application of this procedure in positive displacement screw machines has been pioneered by Kovacevic and has been presented in (9), (10) and (11). The main challenge in the application of such methods is the construction of the grids required for the deforming rotor domains. The authors are only aware of SCORG©, the software developed in house, as a tool available for this purpose and for this reason it has been utilized in the present study. *Kovacevic et al.,* (10) presented a numerical simulation of a combined screw compressor–expander machine for use in high pressure refrigeration systems. *Kethidi et al.,* (12), conducted further studies on the influence of turbulence modelling on the CFD predictions of local velocity fields in twin screw compressors. Optimization of the discharge port area based on flow behaviour in the discharge chamber has been the main subject of research performed by *Mujic et al., (13) and Pascu et al., (14).*

GL-51.2 is a dry running, unsynchronized twin screw machine designed at TU Dortmund, (6). It has been tested for use as an oil free expander of high pressure air at various operating conditions. The experimental data, obtained from this machine, has been used in the present study to validate the use of 3D transient CFD calculation procedures to predict expander performance.

2   CFD ANALYSIS OF A TWIN SCREW EXPANDER

In a compressor, the rotation of rotors displaces the gas from the low pressure port to the high pressure port with gradual decrease in the contained volume. Expander screw rotors rotate in the opposite direction to compressor rotors in such a way that the gas is displaced from the high pressure port to the low pressure port with gradual increase in volume. Since these two processes more or less mirror each other, the same CFD analysis calculation procedures used for screw compressors, can be applied to expanders. The process of obtaining performance predictions starts with the extraction of the fluid flow domains from a 3D CAD model of the expander components, namely the male and female rotors, casings, the high pressure and low pressure connection flanges and the pipes. The expander fluid domain is decomposed into four main regions namely, the male rotor flow domain, the female rotor flow domain, the suction flow domain and the discharge flow domain. The male and female rotor flow domains are separated by a unique plane defined by a rack as explained in (11). The rotor flow domains are mapped in SCORG© and integrated in the same software, with the numerical grids of the port domains generated by commercial software directly from CAD. This is followed by the simulation setup which comprises importing the integral numerical grid in the CFD solver and definition of the operating parameters and solution schemes. The post processing is usually performed within the CFD solver.
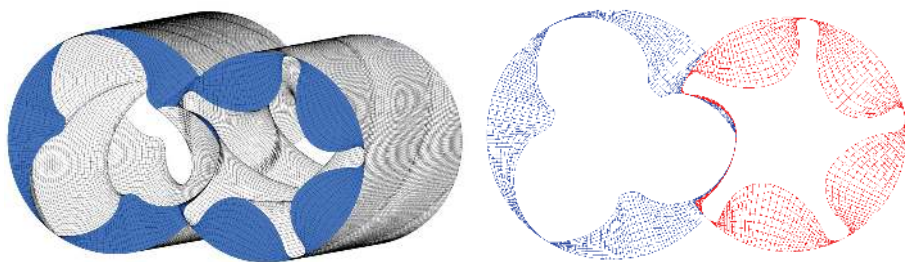

Figure 1. Numerical grid of the GL-51.2 screw expander rotors

GL 51.2 is the twin screw expander designed by TU Dortmund with 3/5 lobe rotor combination. The outer diameters of the male and female rotors are 71.847 mm and 67.494 mm respectively. The L/D ratio is 1.406 and the centre distance between the rotors is 51.222 mm. The male rotor wrap angle is $\Phi_w = 200°$.

2.1   Grid Generation

SCORG© (11) was used to generate hexahedral grid in the rotor domain. The grid of the rotors used in this research is comprised of 40x8x40 divisions in the circumferential, radial and axial direction per interlobe respectively in the male and female fluid zones. The complete rotor grid for one of the cross section is shown in Figure 1.

The mesh in the high and low pressure ports is tetrahedral and generated by use of the ANSYS grid generator. These three domains were assembled together in the solver through non-conformal GGI interfaces. The connecting pipes were meshed by a hexahedral grid. All the domains were integrated to form a single working domain which represented all the flow domains, including the leakage paths through the interlobe and radial leakage gaps. Figure 2 shows the complete model of the analysed expander with all flow sub domains.

Initially, the end clearance leakage area was not included in the calculation but after preliminary evaluation it was noticed that this leakage area plays important role in the performance of the machine. Therefore a hexahedral numerical grid with 5 cells across its thickness was introduced in the model to account for that leakage.
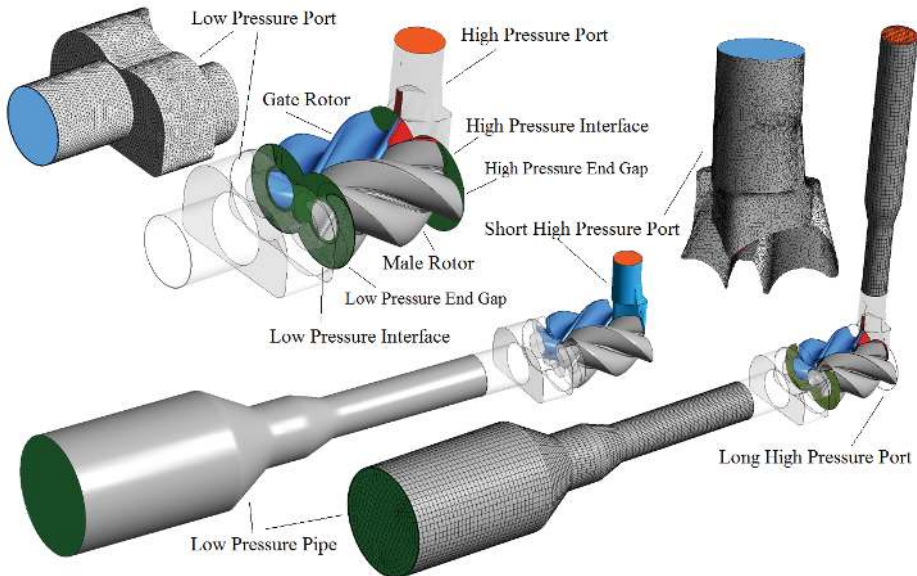

Figure 2. Flow domains for analysis of a twin screw expander

The numerical grid for screw compressor rotors was comprised of 213328 cells. The numerical grid for short ports accounted for 574813 cells while for the long ports it was 585761 cells. The overall number of computational numerical cells with short ports was 788141 while with the long ports it was 799089.

2.2 Simulation

A detailed description of the principles of the CFD simulation of flow in twin screw machines, based on grid generation with SCORG©, can be found in (11). Numerical grids for all time steps are generated in advance of the CFD calculation and are passed to the solver initially in the model setup. At each time step the mesh for the appropriate position of the rotors (Figure 1) is updated in the solver by use of an external subroutine. The solver is set with a higher order advection scheme and the second order backward Euler temporal discretization. The working fluid was air following an ideal gas law with a molar mass of 28.96 kg kmol^{-1}, Specific Heat Capacity 1004.4 J kg^{-1} K^{-1}, Dynamic Viscosity 1.831x10^{-5} kg m^{-1} s^{-1} and Thermal Conductivity 2.61x10^{-2} W m^{-1} K^{-1}.

The convergence criteria for all equations were set to 1.0x10^{-3} applying 10 coefficient loops for every time step. During solution, r.m.s residuals for all time steps achieved values between 1.0x10^{-3} and 5.0x10^{-3} for the momentum equation, while the values for the continuity and energy equations were always less than 1.0x10^{-3}. The calculations were allowed to run for a sufficient number of time steps in order to ensure that cyclic repetition of the flow and pressure values was achieved at the boundaries.

The analysis was carried out in two stages. The objective of the first stage was to identify the modelling parameters that influence the prediction of results from the CFD calculations and select those parameters that provide best results in comparison with experimental data. The main objective of the second stage was to calculate the machine performance, using a selected set of modelling parameters, obtained from the first stage, which best coincided with measured test results.

2.2.1 Stage I: Selection of modelling parameters

The accuracy of performance predictions with CFD model depends on many factors which are dependent on the level of assumptions introduced in the setup. The first phase in analysing this screw expander was to determine the influence of modelling parameters such as:

i) Size of clearance gaps,
Clearance gaps have a significant effect on the performance of screw machines. It was noticed in previous studies (11) that they affect the fluid flow much more significantly than the pressure distribution in the working domain. Three different clearance gaps were evaluated namely the interlobe, radial and end face. The design clearances of this machine were defined as 50-80 μm in the interlobes, 80 μm radially, 100 μm at the high pressure end and 250 μm at the low pressure end. Due to thermal deformation and bearing clearances, these gaps change during the operation of the machine. In order to evaluate the effects of individual gaps on the performance, a number of different values for each of these gaps were compared.

ii) Location of the domain boundary,
Figure 2 shows a model of the screw expander with short and long domains on the suction and discharge ends of the machine. It was expected that the length of the ports and location of boundaries might affect the solution.

iii) Type of boundary condition,
Due to the cyclic variation of pressure, temperature and other values of the flow in the compressor ports, it is difficult to define fixed conditions at the boundaries of the flow domain. Usually it is possible to define an "opening" boundary with a specified non-reflecting pressure head at the boundary location. This type of boundary permits the flow to enter and leave the computational domain but affects the solution, depending on the location of the boundary relative to the source of the pulsations. An alternative approach, proposed in (11), is to define a computational domain at the end of the machine flow domains which will account for a mass and

energy source or sink to simulate constant conditions in the machine reservoirs. Such a source domain adds to or removes mass and energy from the gas so that pressure oscillations in the ports are damped and maintained at a given level.

iv) Flow regime, Laminar or Turbulent simulation,
Flow calculations assuming both laminar flow and the Spalart-Allmaras turbulence model have been checked in various test cases to evaluate their influence on the results. The Spalart-Allmaras turbulence model (12) is a one-equation model that solves a modeled transport equation for the kinematic eddy (turbulent) viscosity. It will be shown that the turbulence modelling influences the mass flow through the expander.

The designed operating speed range of the expander was from 2000 to 16000 rpm. Hence two points at 4000 and 10000 rpm were selected for *Stage I* calculations. Similarly the high end port pressure can range from 1.5 to 3.0 bar, hence a Pressure of 2.0 bar was selected. The results obtained were compared with the measured pressure variation inside the working chamber presented in a Pressure – Alfa diagram. Details of the cases analysed are given in Table 1.

Table 1. Cases evaluated for the analysis in *Stage I*

Case No	High Pressure Port	Male Rotor Speed		High Pressure Boundary	Turbulence	Clearance (um)			
		rpm	rpm			Interlobe	Radial	HP End	LP End
1	Short	4000	10000	Opening Pressure	Spalart-Allmaras	50	80	400	0
2	Short	4000	10000	Opening Pressure	Spalart-Allmaras	50	80	100	0
3	Short	4000	10000	Opening Pressure	Spalart-Allmaras	50	80	100	250
4	Short	4000	10000	Opening Pressure	Spalart-Allmaras	10	10	0	0
5	Long	4000	10000	Opening Pressure	Spalart-Allmaras	50	80	100	0
6	Short	4000	10000	Opening Pressure	Laminar	50	80	100	0
7	Long	4000	10000	Source Domain	Spalart-Allmaras	50	80	100	0

2.2.2 Stage II: Performance evaluation
In the second stage, the CFD models, with setup conditions selected from *Stage I,* were analysed to evaluate the performance of the expander over a wide range of operating conditions.

Experimental values of flow and power, together with the corresponding pressure history inside the machine, as obtained from the TU Dortmund expander test rig are given in (15). The relevant test results, thus obtained are presented in Table 2.

Table 2. Experimental test results for Expander GL 51.2

Speed	2000 rpm		5000 rpm		10000 rpm	
Pressure	Flow rate [kg/s]	Power [W]	Flow rate [kg/s]	Power [W]	Flow rate [kg/s]	Power [W]
1.6 bar	0.0292	511.93	0.0451	1318.84	0.0615	1748.06
2.0 bar	0.0327	758.50	0.0511	1817.65	0.0786	3444.82
3.0 bar	0.0409	1492.35	0.0737	3589.64	0.1179	7148.29

All measured points were taken at a high pressure air temperature of 350° K.

3 RESULTS AND DISCUSSION

3.1   Pressure – Alfa Diagram

A specimen Pressure – Alfa diagram, presented in Figure 3, shows the phases in the expansion process. The working cycle starts with filling, which is characterised by an increase in the volume formed between the rotors exposed to the high pressure port. This part of the process is characterised by pressure fluctuations resulting from the moving rotor and gas interaction. The inlet port of the machine has a relatively small area which results in throttling losses and a pressure drop in the expander inlet. The inlet area initially increases but it then decreases sharply, causing a further pressure reduction in the suction process which is defined as pre-expansion in the diagram.
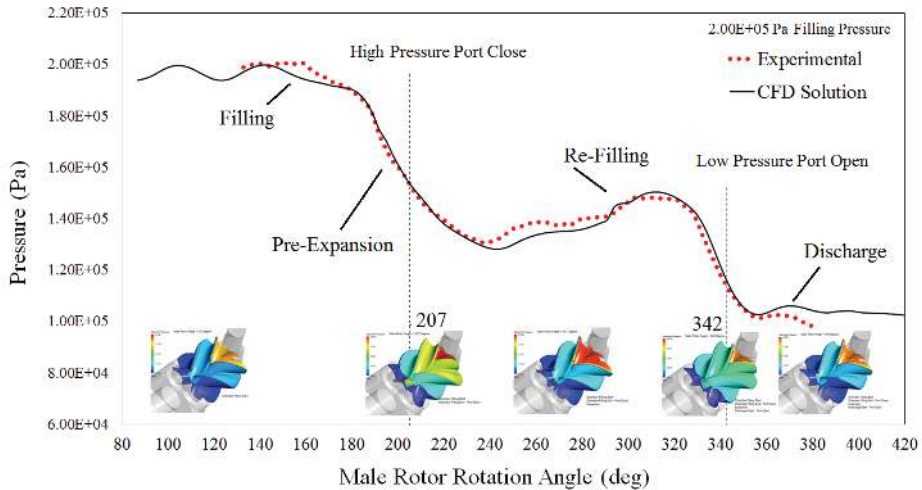

Figure 3. Diagram of indicated pressure in a Twin Screw Expander

Pre-expansion reduces the pressure and hence the generated power. Useful work is produced during the expansion of the gas trapped in the enlarging working chamber. As expansion proceeds, the mass in the working chamber increases due to leakage flow from adjacent chambers which are at higher pressure. If the leakage paths are sufficiently large, this gain in mass can induce a pressure rise in the working chamber, despite its increasing volume. This process is referred to as re-filling and affects the expander power output. The final phase of the process is discharge. Ideally, this should start with the pressure in the working domain near the pressure downstream of the machine.

3.1.1 *Influence of the clearance size on the performance of the expander*

Figure 4 shows the P-Alfa diagram for an inlet pressure of 2.0 bar and an expander speed of 4000 rpm, with various sizes of clearance gaps. It is shown that the size of clearance gaps does not significantly affect pressure during the filling, pre-expansion and discharge phases. However, it has a significant effect on the re-filling process. The nominal clearances specified in the design of this machine are: Interlobe 50 µm, Radial 80 µm and Axial 100 µm. To evaluate their influence on the performance, the following cases were calculated. In Case 1, both the interlobe and the radial clearances were assumed to have their design value, but the axial clearance on the high pressure side was assumed to be 400µm. This case, with deliberately over-specified clearances, produced a P-Alfa diagram close to that of the experiment, but resulted in a very high mass flow rate and a very low indicated specific power. The small clearances assumed in Case 4 inhibited the leakage and

thus reduced the mass flow through the expander, thereby increasing the specific power output. The design values were assumed for interlobe, radial and high pressure axial clearances in Case 2 but zero axial clearance was taken for the low pressure end. This predicted the mass flow rate and specific power well but under predicted the pressure in the re-filling phase. Case 3 with the same interlobe and radial gaps as in Case 2, but with a 250 μm axial low pressure clearance gap also predicted a similar re-filling pressure, with a nearly equal mass flow rate. These cases and several others, not presented in the paper in order to maintain clarity, confirmed that the axial clearance on the high pressure end makes a significant contribution to the direct leakage which increases the mass flow rate through the machine. The axial clearance on the low pressure end, although contributing to the internal leakage, does not affect the mass flow rate through the machine.
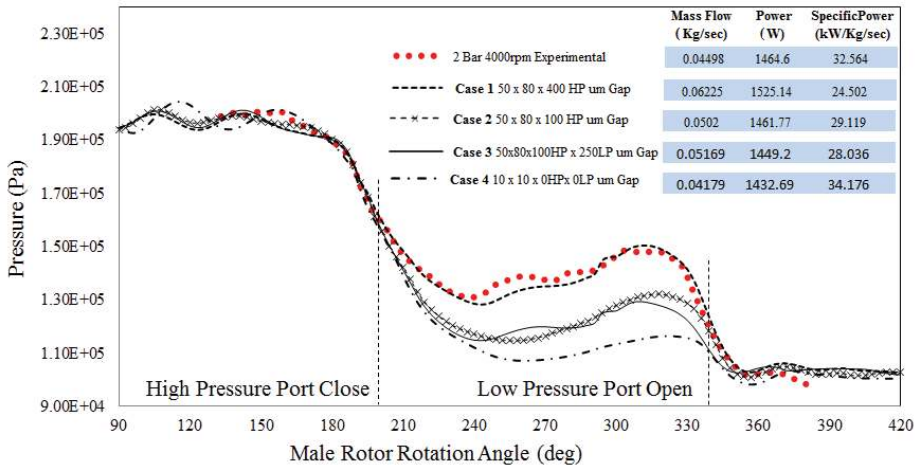

Figure 4. Influence of clearance variation on P-Alfa at 4000rpm
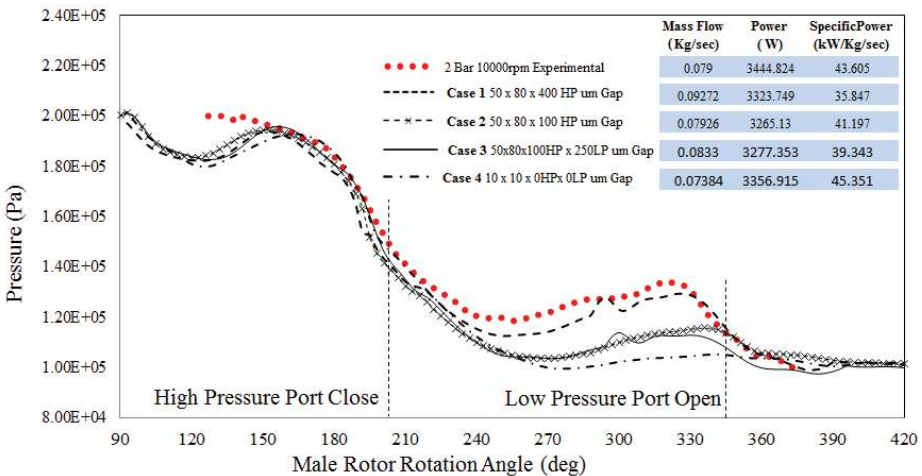

Figure 5. Influence of clearance variation on P-Alfa at 10000rpm

The diagram for 2.0 bar filling pressure and 10000rpm is shown in Figure 5. It is clear from this that the influence of the clearance gaps is larger at lower speeds but it was also noticed that the increase in the interlobe and radial leakage gaps

significantly increases mass flow rate through the machine. The design clearance gaps in Case 2 were selected for further analysis of the machine performance in stage II since they gave the best agreement with the test results in terms of predicting mass flow rate, indicated power and the P-Alfa diagram at both speeds.

As usual, the area under the pressure-volume diagram gives the indicated power, which has been used for comparison in this paper. Although the measured and estimated mass flow rates and indicated powers in Case 2 agree well, the measured refilling pressure is higher at both speeds. This can be explained by the dominant influence of the high pressure region on the indicated power due to the steep change in trapped volume and high pressure level. Therefore it appears to be vital to select operating clearances which will result in an accurately predicted mass flow rate rather than to closely match the pressure curve in the refilling process. It appears that these clearances coincide with the design clearances. However, during the operation of the machine, these clearances will certainly change and will result in different machine performance. The authors are of the opinion that some of the clearance gaps change in such a way that the refilling process does not affect the main mass flow as it occurs after the high pressure port is closed. Further investigation by use of Fluid-Solid Interaction studies may be useful to validate this theory.

3.1.2 Influence of the length of high pressure ports on performance

The P-Alfa diagrams shown in Figure 6 are obtained with different lengths of high pressure ports for the 4000 and 10000rpm studies. The arrangements for the long and the short ports are shown in Figure 2. The long ports place the boundary condition far upstream of the inlet to the rotor filling. This produces pressure fluctuations in the filling process. These fluctuations are not noticeable in the experimental results. On the other hand, the short ports in which the boundary is placed much closer to the expansion chamber provide better predictions of the filling and pre-expansion phase and this results in a much closer match with the test results. Hence the short high pressure ports were selected for *Stage II* calculations.
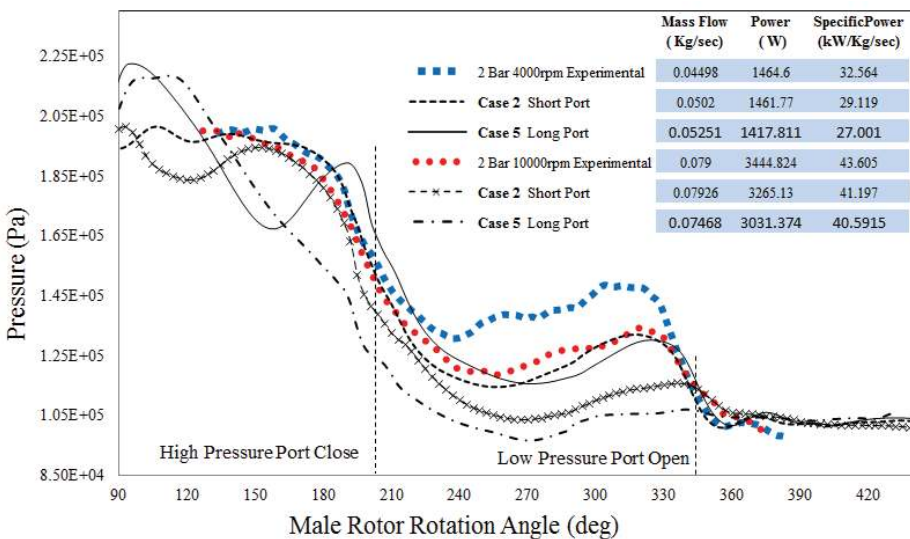

Figure 6. Influence of the location of high pressure boundary on P-Alfa

3.1.3 Setting boundary conditions for the high pressure inlet

Previous authors (11) described the use of a boundary domain for providing quick and stable calculation of the performance of screw compressors. A similar approach was applied to evaluate the expander performance and was compared with non-reflecting pressure boundary conditions at the high pressure opening. Figure 7 shows a comparison between the estimated P-Alfa diagrams and the test results, with two different types of boundary conditions at the high pressure inlet side. The introduction of a source domain caused damping of the pressure fluctuations in the filling stage. Since non-reflecting pressure boundary conditions at the short port openings gave better predictions of both power and mass flow, these were selected for all further performance calculations.
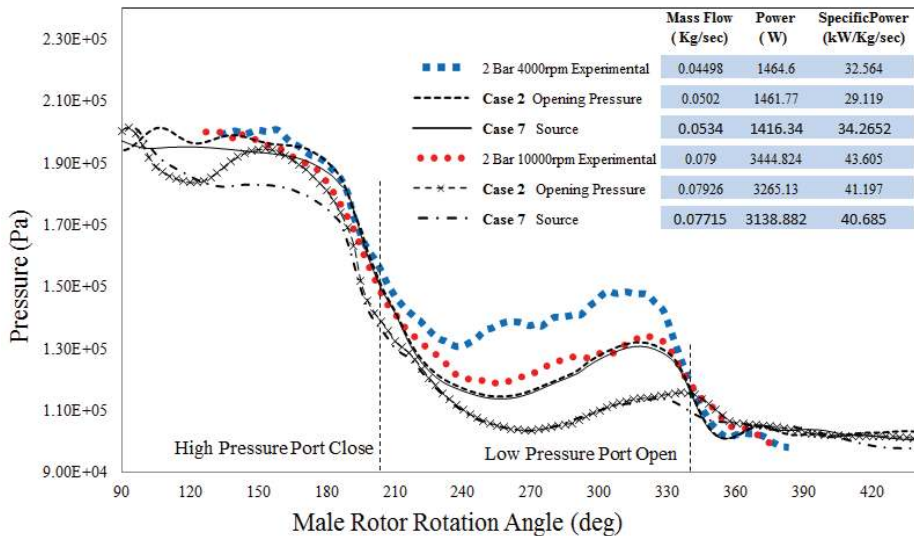

Figure 7. Influence of high pressure boundary condition on P-Alfa

3.1.4 Influence of the Turbulence model

Figure 8 shows P-Alfa diagrams of predicted performance at 4000 and 10000 rpm for both laminar flow and turbulent flow, based on the Spalart-Allmaras model, compared with test results. The inclusion of turbulence reduces the leakage flows and increases the power, thus indicating that it plays a role in clearance flows. Based on the values of power and flow, also given in Figure 8, the Spalart-Allmaras turbulence model was used for all further calculations. Comparing the results in Figure 8 with those in Figure 4, it can be seen that leakage flow and power output are far more sensitive to the size of the clearance gaps than to turbulence effects since the Pressure-Alfa diagram is significantly affected by clearance gap changes but only slightly by the inclusion of turbulence.
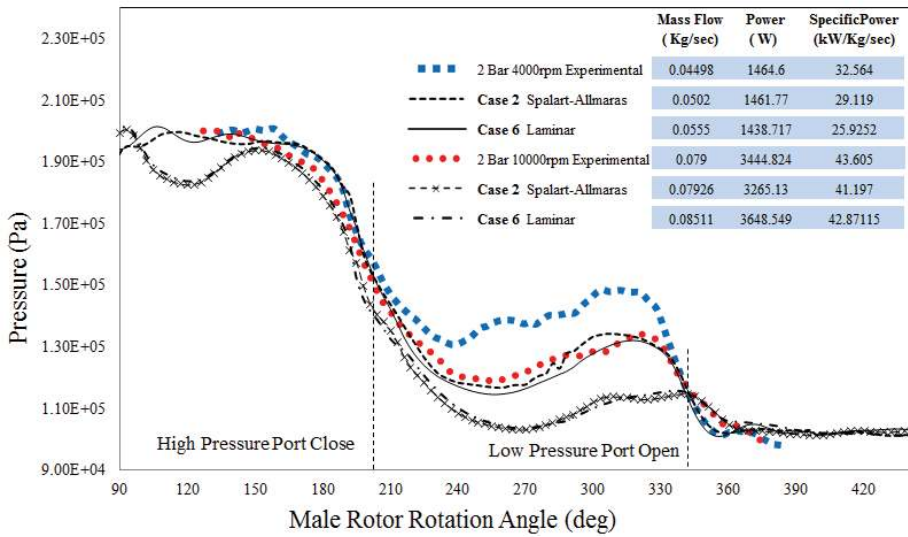
The table shown within the figure:

	Mass Flow (Kg/sec)	Power (W)	SpecificPower (kW/Kg/sec)
■ ■ ■ 2 Bar 4000rpm Experimental	0.04498	1464.6	32.564
- - - **Case 2** Spalart-Allmaras	0.0502	1461.77	29.119
—— **Case 6** Laminar	0.0555	1438.717	25.9252
● ● ● 2 Bar 10000rpm Experimental	0.079	3444.824	43.605
-×-×- **Case 2** Spalart-Allmaras	0.07926	3265.13	41.197
-·-·- **Case 6** Laminar	0.08511	3648.549	42.87115

**Figure 8. Influence of Laminar and Turbulence model on P-Alfa**

3.2   Mass flow rate and Indicated Power

Estimated mass flow rates and indicated power outputs for the cases studied, compared with measured values, are shown in Figure 9 and 10 respectively. These were obtained with the same modelling conditions i.e. short high pressure port, opening pressure boundary condition, the Spalart-Allmaras turbulence model and a clearance distribution of 50μm interlobe, 80μm radial and 100μm axial clearance on the high pressure side and no axial gap on the low pressure side. These show good agreement for Case 2 studies at 4000rpm and 10000rpm. These selected modelling parameters were used for further performance evaluation carried out at operating conditions listed in Table 2.
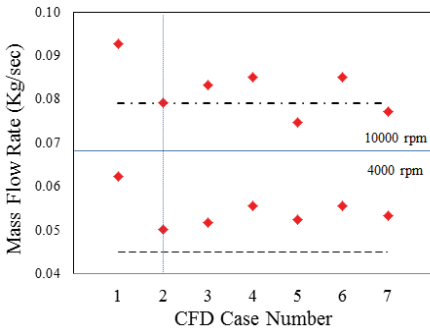
Figure 9. Mass Flow Rate vs CFD Case variants
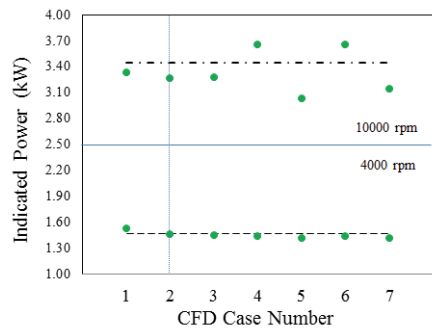
Figure 10. Indicated Power vs CFD Case variants

3.3   Evaluation of overall Performance characteristics

The performance of the expander can be evaluated by comparing the indicated power and mass flow rate with test results at the operating speeds and operating pressures given in Table 2. The results obtained from *Stage II* CFD calculations are presented in Table 3 for the respective operating conditions.

426

Table 3. CFD model performance prediction of GL 51.2

Speed	2000 rpm		5000 rpm		10000 rpm	
Pressure	Flow rate [kg/s]	Power [W]	Flow rate [kg/s]	Power [W]	Flow rate [kg/s]	Power [W]
1.6 bar	0.0297	435.531	0.0425	993.606	0.0621	1690.72
2.0 bar	0.0395	759.192	0.0551	1793.303	0.0794	3265.13
3.0 bar	0.0622	1594.74	0.0852	3877.391	0.1215	7361.67

All calculated points assume the high pressure air temperature to be 350° K.

The estimated performance characteristics of the expander in terms of indicated power and mass flow rate versus male rotor speed at different filling pressures are shown in Figures 11 and 12 respectively. The trends obtained by CFD modelling vary progressively and follow those of the experimental results.
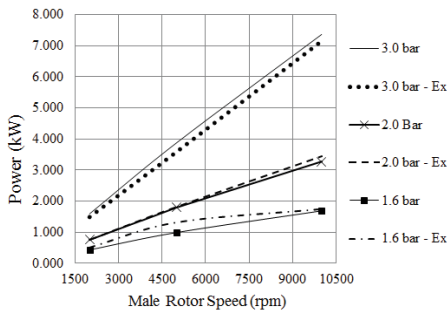

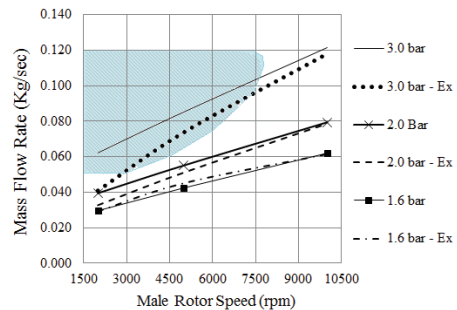**Figure 11. Power vs Speed at different filling pressures**

Figure 12. Mass Flow Rate vs Speed at different filling pressures

These characteristics represent the following:
- The indicated Power increases with both higher rotor speeds and filling pressures. Also, the Specific Power increases at higher pressures. CFD Model predictions of power are relatively over estimated at higher pressure.
- The Mass flow rate increases with both higher speeds and filling pressures, due to the higher gas density in the filling port. CFD Model mass flow rate predictions are very accurate at low pressure but are over estimated at high pressures and Low Speed conditions, where the influence of leakage is higher. This region is highlighted in Figure 12 and further investigation of the CFD models is required to get better results in this regime.

4 CONCLUSION

Transient 3D CFD analysis of a twin screw expander has been successfully carried out using the SCORG© grid generator and ANSYS CFX Solver. In the model setup stage, experimental Pressure-Alfa diagrams were used as a guideline for the selection of appropriate modelling parameters for CFD calculations. In the performance study, a set of different pressure ratios, with different operating speeds at fixed inlet gas temperature were used to validate the established CFD model.

- It is possible to apply the modelling procedures, developed for the analysis of twin screw compressors, to twin screw expanders.
- It is important to define the appropriate geometry and position of the pressure boundary of the high pressure port in order to enable adequate pressure fluctuations and throttling in the port. Further investigation is necessary to generalise this procedure.
- The inclusion of turbulence modelling in CFD calculations does not significantly affect the pressure history within the machine, but it does influence the gap flows and hence the predicted mass flow rate and specific power. The Spalart-Allmaras turbulence model was used in this study but further investigation will need to be performed in order to determine the best turbulence model for screw expanders.
- Clearance distribution in interlobe, radial and axial gaps has a strong influence on the performance of the expander. It is difficult to predict their exact operating values. These were obtained by iterative trials in this case. A comprehensive Fluid-Solid interaction study would help to better understand their dynamic behaviour.

The procedure for the analysis of screw expander developed in this research can be used in future to optimise all aspects of screw expander performance and improve its design.

REFERENCE LIST

(1) Smith I.K, Stosic N, Aldis C A. (1996), *Development of the trilateral flash cycle system, Part3: design of high-efficiency two phase screw expanders*, Proceedings of IMechE, Part A: Journal of Power and Energy, Volume 210.
(2) Smith I.K, Stosic N, Kovacevic A. (2004), *An Improved System for Power Recovery from High Enthalpy Liquid Dominated Field*, GRC Annual Meeting, Indian Wells, California.
(3) Stosic N., Smith I. K., Kovacevic A. (2002) *A Twin Screw Combined Compressor and Expander for CO2 Refrigeration Systems*. Proc. Int. Compressor Conf. at Purdue, pp. C21-2.
(4) Stosic N., Smith I.K., Kovacevic A. (2005) *Screw Compressors: Mathematical Modeling and Performance Calculation,* Springer Verlag, Berlin.
(5) Brummer A., Hutker J. (2009) *Influence of geometric parameters on inlet-losses during the filling process of screw-type motors*. Developments in mechanical engineering, vol. 4, pp. 105-121.
(6) Hutker J., Brummer A. (2012) *Thermodynamic Design of Screw Motors for Constant Heat Flow at Medium Temperature Level*. Proc. Int. Compressor Conf. at Purdue, pp. 1478.
(7) Nikolov A., Huck C., Brummer A. (2012) *Influence of Thermal Deformation on the Characteristics Diagram of a Screw Expander in Automotive Application of Exhaust Heat Recovery*. Proc. Int. Compressor Conf. at Purdue, pp. 1447.
(8) Ferziger J. H., Peric M. (1996*) Computational Methods for Fluid Dynamics,* Springer, Berlin, Germany, third.
(9) Kovacevic A., Stosic N., Smith I. K. (2003) *3-D Numerical Analysis of Screw Compressor Performance.* Journal of Computational Methods in Sciences and Engineering 3: 259-284.
(10) Kovacevic A., Stosic N., Smith I. K. (2006) *Numerical simulation of combined screw compressor–expander machines for use in high pressure refrigeration systems*. Simulation Modeling Practice and Theory 14: 1143–1150.
(11) Kovacevic A., Stosic N., Smith I. K. (2007) *Screw compressors - Three dimensional computational fluid dynamics and solid fluid interaction* Springer-Verlag Berlin Heidelberg New York.
(12) Kethidi M., Kovacevic A., Stosic N., Smith I. K. (2011) *Evaluation of various turbulence models in predicting screw compressor flow processes by CFD*. 7th

International Conference on Compressors and their Systems, City University London.

(13) Mujic E., Kovacevic A., Stosic N., and Smith I. K., (2008) *The influence of port shape on gas pulsations in a screw compressor discharge chamber*, Proceedings of IMechE, Vol. 222 Part E: Journal of Process Mechanical Engineering JPME205.

(14) Pascu M., Kovacevic A., Udo N. (2012) *Performance Optimization of Screw Compressors Based on Numerical Investigation of the Flow Behaviour in the Discharge Chamber*. Proc. Int. Compressor Conf. at Purdue, pp. 1145.

(15) Hütker J., Brümmer A., (2013) *Physics of a dry running unsynchronized twin screw expander*, International Conference on Compressors and their Systems, City University London.